A physically consistent and numerically robust k-ϵ model for computing turbulent flows with shock waves

Pratikkumar Raje, Krishnendu Sinha*

Indian Institute of Technology Bombay, Mumbai, 400076, India

Abstract

High-speed turbulent flows with shock waves pose significant challenge in terms of physical modeling and numerical accuracy. In this paper, we develop a k-ϵ turbulence model for canonical shock-turbulence interaction, based on the physical ideas of shock-unsteadiness damping. The shock-unsteadiness k-ϵ model proposed earlier by Sinha et al. (Phys. Fluids, 15(8), 2003) has model parameters that are functions of upstream Mach number. Our main objective is to eliminate the dependence of the model parameters on upstream flow quantities, and thus overcome difficulties in numerical implementation in complex flow applications. For the turbulent kinetic energy, this is achieved by proposing a new model for the shock-unsteadiness source term that is physically and dimensionally consistent with the earlier formulation. An alternate form of the dissipation rate equation is also used to eliminate upstream dependence of the model parameter in the production term. The proposed model is employed to compute the canonical interaction of a normal shock with homogeneous isotropic turbulence. Large numerical error at the shock wave are eliminated by employing a transformation of the turbulence variables that result in a conservative form of the governing equations. The new model thus gives physically consistent and numerically accurate results at shock waves. The model predictions for turbulent kinetic energy and its dissipation rate are found to match DNS data over a range of Mach numbers.

Keywords: shock/turbulence interaction, shock-unsteadiness, turbulent kinetic energy, turbulent dissipation rate, conservative formulation, RANS

1. Introduction

Interaction of turbulence with shock waves is important in many technological applications in high-speed flight [1–3] and Inertial Confinement Fusion [4–6]. In the case of the high-speed aerospace vehicles, shock-turbulent boundary layer interaction (STBLI) can be found on deflected control surfaces, in front of a vertical fin, and in air-breathing engine inlet ducts. Shock interacting with a turbulent boundary layer enhances the turbulence intensity, which amplifies mixing and dissipation of turbulent kinetic energy. This causes a decrease in the stagnation pressure, resulting in the decrease in vehicle's efficiency due to the significant increase in drag. STBLIs can also cause a sudden increase in pressure, leading to boundary-layer separation and high localized heat loads on the vehicle's surface. Thus, STBLIs limit the vehicle's performance and can also cause structural damages, making its prediction imperative for the design of high-speed vehicles.

Numerical predictions of STBLI flows in practical high-speed applications are generally carried out using Reynolds-averaged Navier-Stokes (RANS) framework [7, 8]. In this approach, the mean flow field is computed and the effect of turbulent fluctuations on the mean flow is introduced using a turbulence model. For the cases involving interactions of strong shock waves with turbulent boundary layers, where boundary-layer separation occurs, conventional turbulence models like k-ϵ, k-ω and Spalart-Allmaras perform poorly [2, 9, 10]. Significant errors in the predictions of the size and location of the separation region, surface pressure and heat-transfer rates are observed. Majority of the research work [11–17] has therefore been directed to improve the performance capabilities of these models in STBLI flows. A detailed discussion about the latest trends and challenges can be found in Gaitonde [18], Zheltovodov [19] and Dolling [20]. Non-linear eddy viscosity models have also been applied to STBLI flows to address some of the limitations of the linear formulation based two equation models like k-ϵ and k-ω [21–23].

The standard k-ϵ model predicts a very high amplification of turbulence kinetic energy (TKE) compared to direct numerical simulation (DNS) data across a shock [24, 25]. The over-amplification of TKE is due to the excessive production of turbulence at the shock wave. Sinha et al. [24] argues that one of the main reasons for the high level of turbulence production is the breakdown of eddy-viscosity assumption in the highly non-equillibrium region of a shock wave. A realizable model [17, 26] suppresses eddy-viscosity and brings down the post-shock turbulence level, but the predictions are still appreciably higher than the DNS data. Setting eddy viscosity to zero in the shock wave matches DNS data for weak shocks, but the predictions are still too high for strong shock waves. This is possibly because of the additional physics that is not included in the con-

*Corresponding author
Email address: krish@aero.iitb.ac.in (Krishnendu Sinha)

ventional models. The standard k-ϵ model along with its other variants mentioned previously neglect the inherent unsteady nature of a shock wave due to turbulent fluctuations.

Sinha et al. [24] study the physics of the unsteady motion of a shock wave and suggest improvements in the standard k-ϵ model. The turbulent kinetic energy k equation is modified to include a term due to shock-unsteadiness, which is modeled using linear interaction analysis. This term represents the damping effect of shock oscillations on the amplification of TKE. The dissipation rate ϵ equation is similarly altered based on the linear theory results. Modifications in the k and ϵ equations result in the model parameters to be functions of the upstream Mach number normal to the shock. This dependency of the model parameters on the upstream flow variables arises due to the two basic underlying assumptions used to model the shock-unsteadiness effect:

(a) unsteadiness of shock is caused by turbulent fluctuations in the upstream flow and

(b) amount by which shock experiences unsteady motion depends on shock strength and hence the upstream Mach number M_1.

These are fair assumptions considering that the physics of shock-turbulence interaction depends significantly on the strength of the shock wave and incoming turbulence.

Application of the shock-unsteadiness model to STBLIs has been successfully carried out in the recent past. The model has been tested in supersonic compression corner flows [9] and the results were compared with the experimental data of Settles and Dodson [27]. The results show significant improvement over conventional models in predicting the separation-shock location, flow separation and reattachment and surface pressure distribution. Likewise, for oblique shocks impinging on a turbulent boundary layer [28] and cone-flare configurations [16], the shock-unsteadiness model shows similar improvement. The size of the separation bubble and the wall pressure distribution match the experimental data better than the standard models. The flow topology in the interaction region, in terms of the pattern of shocks and expansion waves, is predicted correctly by the modified turbulence model.

Implementation of the shock-unsteadiness k-ϵ model to STBLI flows is non-local in nature. To solve the model equations at points in a shock region therefore requires information about the flow variables at points upstream of the shock wave. A procedure to evaluate the shock-normal Mach number at points upstream of a shock wave is presented in [9]. The upstream direction is identified by the local streamline, and velocity and temperature at an upstream point outside the shock is used to compute the Mach number. The direction of the shock wave is then obtained in terms of the local mean pressure gradient, and is used to compute the component of the upstream Mach number normal to the shock wave.

The boundary layer gradients often result in curved shock waves in STBLIs, and evaluating the upstream shock-normal Mach number along a curved shock is a non-trivial exercise. The process is further complicated in the presence of multiple shock waves and shock-shock interactions, as in the hypersonic cone-flare configurations [16] and oblique shock impingement case [28]. Thus, the dependency of the model parameters on M_1 and hence the non-local nature of the model equations makes it difficult and cumbersome to apply the shock-unsteadiness k-ϵ model in realistic CFD simulations.

The objective of the present work, which builds on the existing physics-based shock-unsteadiness turbulence model, is to develop a physically consistent and numerically robust k-ϵ model for shock-turbulence interaction. This is done by eliminating the dependence of model parameters on the non-local upstream flow parameters, as is the case for the shock-unsteadiness model [24]. The turbulence source terms in the proposed model are functions of the local flow variables at a given grid point. We also cast the new model equations in a conservative form to avoid large numerical error at flow discontinuities. As shown in [29], non-conservative source terms can result in unrealistic CFD results at shock waves, and the predictions are qualitatively and quantitatively different from the analytical solution of the governing equations. Further, we attempt to retain the physical characteristics of the problem and maintain the accuracy of the shock-unsteadiness model with respect to DNS data of shock-turbulence interactions.

The paper is organised as follows. The canonical interaction of homogeneous isotropic turbulence with a normal shock wave is taken as the model problem and is described in section 2. This is followed by turbulence model equations in section 3 for the shock-unsteadiness k-ϵ model [24] developed using the physics of shock-turbulence interaction. Next, we develop new forms of the k and ϵ equations in section 4 that are physically and dimensionally consistent, and numerically more robust than the earlier model. The new model is used to compute a series of shock-turbulence interaction cases and the predictions are compared with the existing DNS data. The numerical procedure and the results are presented in section 5 and 6 respectively.

2. Canonical shock/turbulence interaction

The canonical interaction of homogeneous isotropic turbulence with a nominally normal shock is the model problem

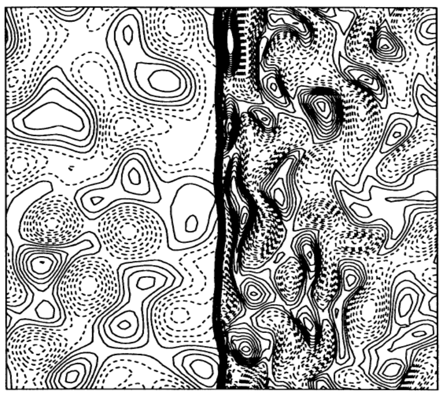

Figure 1: A snapshot of transverse vorticity contours from DNS of a Mach 2 canonical shock/turbulence interaction showing turbulence amplification and shock wave undulations (Reproduced from [31]).

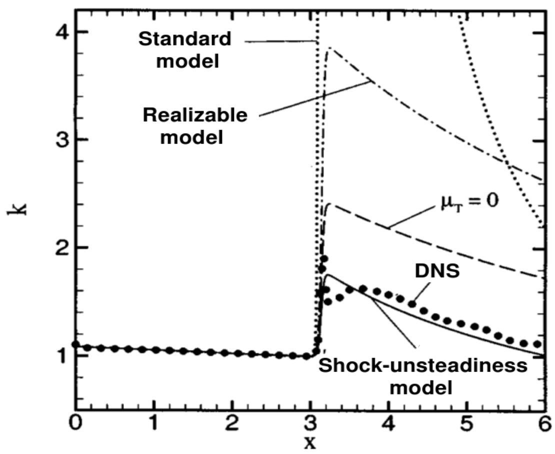

Figure 2: Streamwise evolution of TKE in a Mach 3 shock/turbulence interaction obtained using DNS and different turbulence models (Reproduced with permission from [24]. Copyright [2003], AIP Publishing LLC).

considered in this work. The modal description of compressible turbulence proposed by Kovasznay [30] is used, and the incoming turbulence is considered to consist of purely the vortical mode. Fig. 1, taken from [31] with permission, shows an instantaneous snapshot of the turbulent vortical structures interacting with a Mach 2 normal shock wave. The mean flow is from left to right; it is one-dimensional, uniform and steady. The jump in the mean flow quantities across the shock is governed by the Rankine-Hugoniot relations. Turbulence gets amplified across the shock wave and the amplification in the turbulence quantities, i.e., TKE and its dissipation rate, is proportional to the gradients in the mean flow variables. The amplification of the turbulent vorticity fluctuations across the shock is visible in Fig. 1. The shock wave shows unsteady oscillations due to the passage of turbulent fluctuations through it.

The model problem simplifies the mean conservation equations as well as the turbulence model equations considerably. Complexities due to the boundary-layer velocity gradients, flow separation, streamline curvature, which are encountered in STBLI flows, are not involved. However, the model problem exhibits a range of physical effects, like unsteady shock oscillations, amplification of TKE across the shock, high heat transfer rates in the shock-turbulence interaction region, etc. The main aim of investigating such a flow is to isolate the net effect of the strong gradients of mean quantities imposed by the shock wave on the turbulence. Such studies provide important insights into the underlying physics of shock-turbulence interaction. It can serve as a building block flow, from which information about the physical interactions could be applied to the modeling of more complex inhomogeneous flows.

The canonical shock/turbulence interaction (STI) has been the subject of study for almost half a century and extensive DNS studies have been carried out, e.g. Hannappel et al. [32], Lee et al. [31, 33], Mahesh et al. [34], Jamme et al. [35], Larsson et al. [36, 37]. These studies mainly focus on understanding the physics of the shock-turbulence interactions. They provide qualitative and quantitative information about the Reynolds stresses, TKE and vorticity amplifications, and variations in turbulence length scales, temperature and density variances across the shock. Fig. 2 presents a sample DNS data of TKE variation in a Mach 3 shock-turbulence interaction. The turbulent Mach number and the Reynolds number based on the Taylor microscale are 0.11 and 19.7 respectively. The shock is located at $x = 3$, and the TKE is normalized by its values immediately upstream of the shock. The TKE upstream of the shock decays from its inlet value, due to the absence of mean velocity gradients. There is an amplification in its value across the shock, followed by a faster decay due to the increase in the turbulent dissipation rate at the shock. A rapid non-monotonic variation is observed immediately behind the shock and it corresponds to the acoustic adjustment region, as described by Mahesh et al. [34]. Several turbulence model predictions are compared with the DNS data in Fig. 2 and they are discussed subsequently.

Theoretical tools like linear interaction analysis (LIA) and rapid distortion theory are also well developed to study the shock-turbulence interaction problem. The rapid distortion theory only accounts for a homogeneous mean flow compression, whereas LIA includes vorticity and TKE generation due to shock-front distortion and unsteady oscillations, along with the mean flow compression. Thus, LIA is a closer representative to the flow physics [38] and is based on the inviscid assumption of the flow [39]. The upstream turbulence is decomposed into Kovasznay modes. Linearised Euler equations are then solved downstream of the shock-wave, with linearised Rankine-Hugoniot relations applied at the shock. The solution gives the amplifications of TKE, fluctuating vorticity and thermodynamic fluctuations at the shock wave. Fig. 3 shows amplification in the TKE across the shock as a function of the upstream Mach number, obtained using LIA [31] and DNS [36]. Both the DNS and LIA results show a similar trend; TKE amplification increases till $M_1 = 3$, after which it saturates for higher Mach numbers. DNS results are slightly lower compared to the LIA theory. This is because, DNS solves for the full Navier-Stokes equations, where viscous effects are consid-

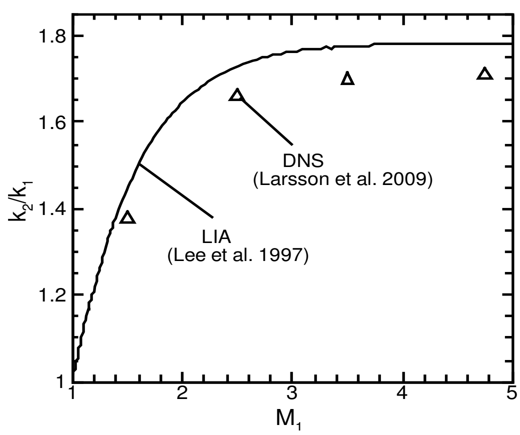

Figure 3: Variation of TKE amplification across a normal shock with upstream Mach number obtained from LIA [31] and DNS [36]; subscript '1' denotes the upstream value and '2' denotes the value downstream of the shock.

ered, that brings down the TKE levels slightly as compared to the inviscid linear theory results.

The understanding of physics together with the availability of extensive DNS data and LIA theory results for the canonical shock/turbulence interactions helps in evaluating existing models and developing new closure models for turbulence correlations of interest. In Fig. 2, the results obtained using the standard and realizable k-ϵ models are evaluated against the DNS data of Lee et al. [31]. As discussed earlier, the results show that the TKE amplification across the shock is overly predicted by these models in comparison with the DNS data. The reason behind this discrepancy can be attributed to the fact that the equilibrium concept of the eddy viscosity breaks down in a highly non-equilibrium flow, such as a shock/turbulence interaction [24]. Supressing μ_T entirely in the shock region by setting it to zero brings down the TKE amplification level, but still a significant overprediction can be seen. A good match with the DNS data is obtained for the shock-unsteadiness k-ϵ model [24] (see Fig. 2), which is developed using the LIA theory results and is discussed in detail in Section 3. Linear theory results have also been used in other modeling works [40, 41] and the ideas have been extended to k-ω and Spalart-Allmaras turbulence models. Application of these physics-based models to complex two-dimensional STBLI flows [9, 16, 28] has also been carried out and successfully validated against available experimental data.

Another important advantage of studying canonical shock/turbulence interaction is in terms of numerical error analysis. Shock-waves are numerical discontinuities and are prone to large numerical error. The simplified one-dimensional mean flow and turbulence model equations for canonical shock/turbulence interactions can be solved analytically, and the closed form exact solutions serve as a benchmark for assessing the accuracy of numerical methods. Sinha and Balasridhar [29] use this approach to quantify the large numerical error in k and ϵ values, when turbulence models are employed in shock-capturing numerical simulations. They propose a new form of the model equations based on a transformation of the turbulence variables to eliminate these errors, and the new approach is able to match analytical results and DNS data closely. A similar analysis of the k-ω turbulence model is presented in [42].

3. Physics based shock-unsteadiness modification to k-ϵ model

The standard k-equation [43] for a compressible steady one-dimensional mean flow through a normal shock simplifies to

$$\bar{\rho}\tilde{u}\frac{\partial k}{\partial x} = -\bar{\rho}\widetilde{u_i''u_i''}\frac{\partial \tilde{u}}{\partial x} - \bar{\rho}\epsilon + \overline{p'\theta'} \qquad (1)$$

where $k = \frac{1}{2}\widetilde{u_i''u_i''}$ is the turbulent kinetic energy, ρ is the density, u is the component of velocity in the stream-wise direction x, p is the pressure and $\theta = \partial u_j/\partial x_j$ is the dilatation. Here, overbar and tilde represent Reynolds and Favre-averaged quantities, and the prime and double-prime represent the Reynolds and Favre fluctuations respectively. The source terms correspond to the production and dissipation mechanisms, where ϵ is a sum of the solenoidal part ϵ_s and the dilatational part ϵ_c. We neglect the viscous and turbulent diffusion terms, as per [24]. The normal Reynolds stress $\bar{\rho}\widetilde{u''u''}$ is modeled using the Boussinesq assumption as

$$\bar{\rho}\widetilde{u''u''} = -\frac{4}{3}\mu_T\frac{\partial \tilde{u}}{\partial x} + \frac{2}{3}\bar{\rho}k \qquad (2)$$

where μ_T is the eddy viscosity and is given by $\mu_T = c_\mu\bar{\rho}k^2/\epsilon_s$ and $c_\mu = 0.09$ is a model constant.

Sinha et al. [24] studies the physics of canonical STI to suggest improvements in the k-ϵ model. A transport equation for k is derived in the reference frame of the shock by assuming that the shock undergoes small deviations from its mean position. The transport equation has an extra term that contains the effect of unsteady shock oscillations. Linear analysis shows that this term has a damping effect on the amplification of TKE through the shock. It is modeled with the assumption that shock-unsteadiness is proportional to the turbulent fluctuations in the flow. The value of the constant of proportionality obtained using LIA results is modified such that TKE amplifications across the shock match the limiting behaviour for $M_1 \to 1$ and $M_1 \to \infty$. Thus, the modeled k-equation takes the form

$$\bar{\rho}\tilde{u}\frac{\partial k}{\partial x} = -\frac{2}{3}\bar{\rho}k\frac{\partial \tilde{u}}{\partial x} + \frac{2}{3}b_1'\bar{\rho}k\frac{\partial \tilde{u}}{\partial x} - \bar{\rho}\epsilon_s \qquad (3)$$

where $b_1' = b_{1,\infty}(1 - e^{1-M_1})$ is called as the shock-unsteadiness damping parameter and $b_{1,\infty} = 0.4$ is its high Mach number limiting value. Notice that the turbulent viscosity is suppressed in the production term so as to minimize the error due to the limitations in the Boussinesq approximation. In the shock region, setting μ_T equal to zero results in the isotropic form of the Reynolds stress, $\bar{\rho}\widetilde{u''u''} = \frac{2}{3}\bar{\rho}k$, which is valid for the shock-upstream flow. In case of the models with realizability constraints [17, 26] and nonlinear eddy-viscosity based formulations [21, 22], the limitations in Boussinesq approximation are taken care of by suppressing the model parameter c_μ in regions of high mean flow gradient. Eq. (3) is applicable to one-dimensional shock-turbulence interactions with uniform mean flow on either sides of the shock wave and represents a significant improvement over the existing models. Compressibility corrections [44], in the form of dilatational dissipation and pressure dilatation, do not improve turbulence levels significantly [24]. Further, they deteriorate model predictions in the upstream boundary layer and therefore are not preferred in STBLI flows [45]. Hence, they are not included in Eq. (3).

The solenoidal dissipation rate ϵ_s is defined as the product of the mean kinematic viscosity $\bar{\nu}$ and enstrophy, i.e., mean-square vorticity fluctuations $\overline{\omega_i'\omega_i'}$, and hence can be written as $\epsilon_s = \bar{\nu}\overline{\omega_i'\omega_i'}$. Sinha [41] assumes that ϵ_s is the dominant part in the turbulent dissipation rate. A transport equation for the evolution of ϵ_s is derived using linearised Navier-Stokes equations and is modeled as,

$$\overline{\rho}\tilde{u}\frac{\partial \epsilon_s}{\partial x} = -\frac{2}{3}c_{\epsilon 1}\overline{\rho}\epsilon_s\frac{\partial \tilde{u}}{\partial x} - c_{\epsilon 2}\overline{\rho}\frac{\epsilon_s^2}{k} \tag{4}$$

where $c_{\epsilon 1} = 1+0.21M_1$ and $c_{\epsilon 2} = 1.2$ are the model parameters. The first term on the right-hand-side brings in the effect of mean compression on the vorticity fluctuations and the effect of temperature rise on the mean kinematic viscosity. It represents the mechanism by which the dissipation rate of TKE gets amplified across the shock. The second term is the dissipation mechanism whose effects are significant only in the shock-free region and can be neglected in the shock wave [24]. It governs the decay rate of turbulence on either sides of the shock wave. Eq. (4) is applicable to the canonical case where homogeneous isotropic turbulence passes through a normal shock and is able to predict the amplification of the TKE dissipation rate accurately. Note that the above form of the model constant $c_{\epsilon 1}$ proposed in [41] is close to that in [24] and using any of the forms makes practically no difference to the results obtained.

4. A new k-ϵ model

The model parameter $b_1^{'}$ in Eq. (3) and $c_{\epsilon 1}$ in Eq. (4) are functions of the upstream Mach number, which makes their numerical implementation non-local on a computational mesh. We attempt to remove this dependency using the following approach.

4.1. Turbulence Kinetic Energy

Across the shock, the conservation of mean momentum can be simplified to

$$\overline{\rho}\tilde{u}\frac{\partial \tilde{u}}{\partial x} + \frac{\partial \overline{p}}{\partial x} = 0 \tag{5}$$

Rewriting the above equation as,

$$\frac{\partial \tilde{u}}{\partial x} = -\frac{\tilde{u}}{\overline{\rho}\tilde{u}^2}\frac{\partial \overline{p}}{\partial x} \tag{6}$$

and assuming that $\overline{\rho}\tilde{u}^2$ scales as $\overline{p}$, we get

$$b_1^{'}\frac{\partial \tilde{u}}{\partial x} = -c\frac{\tilde{u}}{\overline{p}}\frac{\partial \overline{p}}{\partial x} \tag{7}$$

where c is a new model parameter. The above equation gives an alternative model for the shock-unsteadiness term, and leads to a new form of the k-equation,

$$\overline{\rho}\tilde{u}\frac{\partial k}{\partial x} = -\frac{2}{3}\overline{\rho}k\frac{\partial \tilde{u}}{\partial x} - \frac{2}{3}c\overline{\rho}k\frac{\tilde{u}}{\overline{p}}\frac{\partial \overline{p}}{\partial x} - \overline{\rho}\epsilon_s \tag{8}$$

A suitable value of the model constant c is obtained by calibrating it to the shock unsteadiness k-ϵ model [24]. The calibration is done for normal shocks with upstream Mach numbers ranging from 1 to 5.

Integrating Eq. (7) across the shock, we get

$$b_1^{'}ln\left(\frac{\tilde{u}_2}{\tilde{u}_1}\right) = -c\,ln\left(\frac{\overline{p}_2}{\overline{p}_1}\right) \tag{9}$$

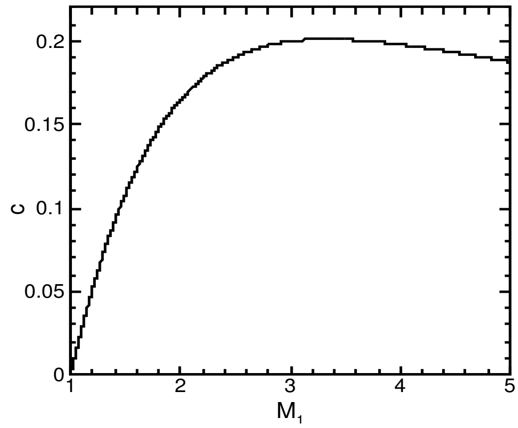

Figure 4: Variation of the model parameter c with upstream Mach number.

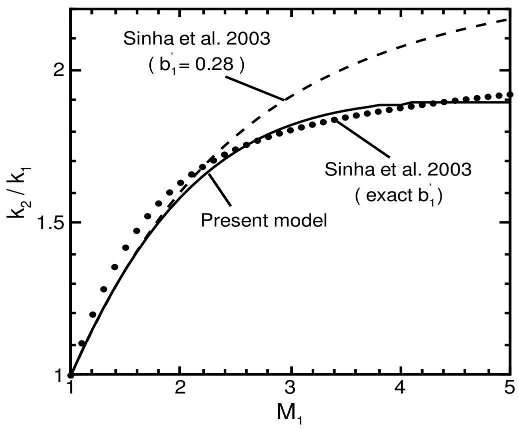

Figure 5: TKE amplification for varying upstream Mach number as obtained for the present model with $c = 0.194$, shock-unsteadiness model [24] with exact $b_1^{'}$ and $b_1^{'} = 0.28$.

Note that the subscripts '1' and '2' denote the values of the quantities upstream and downstream of the shock respectively. Using $b_1^{'}$ and Rankine-Hugoniot jump conditions for $\tilde{u}$ and $\overline{p}$, we obtain the value of c as a function of the shock strength (Fig. 4). The model constant varies between 0 and 0.2 for Mach numbers in the range 1 to 5. A positive c and a positive pressure gradient at the shock results in a negative contribution of the corresponding source term in Eq. (8). Thus, it brings down the amplification of TKE in the shock region. This is physically consistent with the function of the shock unsteadiness modification of Sinha et al. [24]. A value of $c = 0.194$ is recommended as it gives the best possible match with the shock unsteadiness k-ϵ model. Neglecting the TKE dissipation rate in the shock region and integrating Eq. (8) across the shock, we get

$$\left(\frac{k_2}{k_1}\right) = \left(\frac{\tilde{u}_1}{\tilde{u}_2}\right)^{2/3}\left(\frac{\overline{p}_2}{\overline{p}_1}\right)^{-2c/3} \tag{10}$$

Similarly, neglecting the turbulent dissipation from Eq. (3) and

Table 1: Error (in %) in TKE amplification for the present model with $c = 0.194$ and Sinha et al. [24] with $b_1^{'} = 0.28$, computed with respect to the shock-unsteadiness model presented in [24].

M_1	Present Model (c = 0.194)	Sinha et al. [24] ($b_1^{'} = 0.28$)
1.5	− 4.98	− 4.98
2.5	− 0.45	2.5
3.5	1.24	8.79
4.7	− 0.64	12.36
5	− 1.4	12.85

integrating it across the shock yields,

$$\left(\frac{k_2}{k_1}\right) = \left(\frac{\tilde{u_1}}{\tilde{u_2}}\right)^{2(1-b_1^{'})/3} \tag{11}$$

Here, k_2/k_1 represents the jump in TKE across the shock wave. Fig. 5 shows the TKE amplifications across the shock obtained by plotting Eq. (10) for a range of upstream Mach numbers. The results are compared with the TKE amplifications obtained using Eq. (11). With the recommended value of c, the present model underpredicts the TKE amplication upto 5% in the range $1 < M_1 < 2.5$ and slightly overpredicts at higher Mach numbers up to 4.5. Overall, the error with respect to the shock-unsteadiness k-ϵ model of Sinha et al. [24] is less than 5% (See Table 1).

Another approach to make the shock-unsteadiness k-equation local is to choose a constant value of the model parameter $b_1^{'}$ from its range of 0 to 0.4. Fig. 5 shows the TKE amplification obtained using Eq. (11) with a constant value of $b_1^{'} = 0.28$. This constant value is chosen to match with the TKE amplification for $M_1 = 1.5$ obtained using the newly proposed model. Both the shock-unsteadiness k-ϵ and the present model with constant model parameters underpredict TKE amplification by about 5 % at $M_1 = 1.5$. As against the present model, the error in prediction gets significantly larger for the shock-unsteadiness model with constant $b_1^{'}$ as the upstream Mach number increases (See Table 1). Thus, the new formulation improves predictions for a constant model parameter $c = 0.194$ as against taking a constant value of $b_1^{'}$.

4.2. Turbulent dissipation rate

Similar to $b_1^{'}$ in the TKE equation, the model parameter $c_{\epsilon 1}$ in the solenoidal dissipation rate equation (4) is also a function of the upstream Mach number. To remove this dependency, we take an alternative form of the transport equation for the solenoidal dissipation rate ϵ_s from Sinha [41]. For the sake of completeness, the key steps in the modeling of ϵ_s are discussed below. For a detailed discussion, refer to Sinha [41].

Amplification of ϵ_s across the shock can be expressed in terms of the amplification in enstrophy $\overline{\omega_i^{'}\omega_i^{'}}$ and the changes in the kinematic viscosity $\bar{\nu}$,

$$\tilde{u}\frac{\partial \epsilon_s}{\partial x} = \tilde{u}\frac{\partial}{\partial x}(\bar{\nu}\overline{\omega_i^{'}\omega_i^{'}}) = \tilde{u}\overline{\omega_i^{'}\omega_i^{'}}\frac{\partial \bar{\nu}}{\partial x} + \tilde{u}\bar{\nu}\frac{\partial}{\partial x}(\overline{\omega_i^{'}\omega_i^{'}}) \tag{12}$$

The amplification in enstrophy $\overline{\omega_i^{'}\omega_i^{'}}$ across the shock is modeled using LIA. Linearized Navier-Stokes equations are written in a reference frame attached to the unsteady shock wave to derive transport equations for the vorticity components. These are combined to obtain an equation for the enstrophy evolution across a time-averaged shock wave. A budget of this equation is computed using the results from LIA and DNS data to identify the dominant terms responsible for the amplification of the enstrophy across the shock. Closure approximations are then proposed for the unclosed correlations in the dominant source terms resulting in the following equation.

$$\tilde{u}\frac{\partial}{\partial x}(\overline{\omega_i^{'}\omega_i^{'}}) = -c_w\overline{\omega_i^{'}\omega_i^{'}}\frac{\partial \tilde{u}}{\partial x} \tag{13}$$

where $c_w = 1.55$. This equation governs the production of enstrophy due to the mean flow compression across the shock and is used to derive an equation for ϵ_s.

The dynamic viscosity $\bar{\mu} = \bar{\nu}\bar{\rho}$ is assumed to be a function of mean temperature $\tilde{T}$, such that $\bar{\mu} \propto \tilde{T}^{\alpha}$ where $\alpha = 0.76$ is a constant. The change in kinematic viscosity across the shock can thus be calculated as,

$$\frac{\partial \bar{\nu}}{\partial x} = -\frac{\bar{\mu}}{\bar{\rho}^2}\frac{\partial \bar{\rho}}{\partial x} + \frac{1}{\bar{\rho}}\frac{\partial \bar{\mu}}{\partial x} = \bar{\nu}\left[\frac{1}{\tilde{u}}\frac{\partial \tilde{u}}{\partial x} + \frac{\alpha}{\tilde{T}}\frac{\partial \tilde{T}}{\partial x}\right] \tag{14}$$

Combining Eqs. (13) and (14), we get

$$\bar{\rho}\tilde{u}\frac{\partial \epsilon_s}{\partial x} = (1 - c_w)\bar{\rho}\epsilon_s\frac{\partial \tilde{u}}{\partial x} + \alpha\bar{\rho}\epsilon_s\frac{\tilde{u}}{\tilde{T}}\frac{\partial \tilde{T}}{\partial x} - c_2\bar{\rho}\frac{\epsilon_s^2}{k} \tag{15}$$

where viscous dissipation with $c_2 = 1.2$ is added to match the turbulence decay in DNS data on each side of the shock wave. The first two terms on the right-hand-side of the above equation are responsible for the amplification in ϵ_s across the shock,

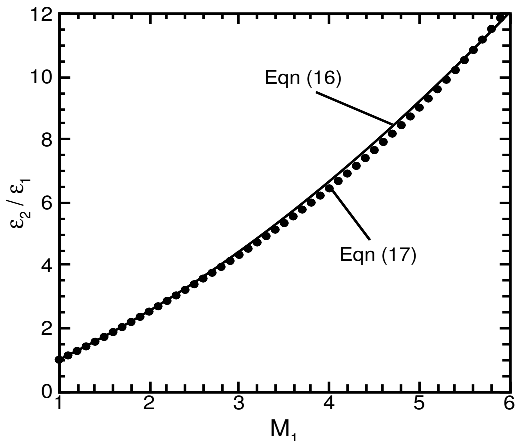

Figure 6: Amplification in the turbulent dissipation rate for different upstream Mach numbers as obtained using Eqs. (16) and (17).

while the last term causes its decay on either sides of the shock wave. The equation neglects the effects due to viscous and turbulent diffusion and can be assumed to hold for high Reynolds number flows.

Analytical values of the amplification in the turbulent dissipation rate in the inviscid limit can be obtained by neglecting the dissipation of ϵ_s from Eq. (15) and then integrating it across the shock,

$$\left(\frac{\epsilon_{s2}}{\epsilon_{s1}}\right) = \left(\frac{\tilde{u_1}}{\tilde{u_2}}\right)^{(c_w-1)} \left(\frac{\tilde{T}_2}{\tilde{T}_1}\right)^{\alpha} \tag{16}$$

Comparing the jumps in the turbulent dissipation across the shock obtained using Eq. (16) and those obtained from Eq. (4),

$$\left(\frac{\epsilon_{s2}}{\epsilon_{s1}}\right) = \left(\frac{\tilde{u_1}}{\tilde{u_2}}\right)^{(2/3)c_{\epsilon 1}} \tag{17}$$

shows that the results are almost identical for a range of upstream Mach numbers (see Fig. 6). Unlike TKE jump, the amplification of turbulent dissipation rate across the shock increases steadily with the increase in the upstream Mach number.

4.3. *Non-conservative errors at a shock wave*

The k and ϵ_s equations given by Eqs. (8) and (15) respectively are non-conservative in nature. This is due to the fact that derivatives in the source terms on the right-hand-side of both the equations are multiplied by the flow variables. Sinha et al. [29] studies the numerical issues involved while solving the non-conservative form of the shock-unsteadiness k-ϵ equations. It is pointed out that for shock capturing simulations, like those in this work, the non-conservative nature of the source terms can result in large numerical error at shock waves. The error can be minimized by casting all the terms in conservative form. The convection terms in the Eqs. (8) and (15) can be written in a conservative form using the Reynolds-averaged mass conservation equation. In a finite-volume approach, the convective fluxes are evaluated at cell interfaces. The corresponding truncation error involves higher-order derivatives of the flow variables. These derivatives take large values in the shock wave, but contributions from adjacent cells cancel at the common interfaces when all the finite volume cells spanning the shock wave are taken together. The net error across a shock wave is therefore a function of the higher-order derivatives evaluated in a region of smooth flow solution, outside the shock wave. On successive grid refinement, the leading-error term vanishes and the solution tends towards the exact integral. A detailed numerical error analysis at the shock wave can be found in the Appendix of [29] and is not repeated here.

The source terms in both the k and ϵ_s equations involve flow derivatives that are evaluated using a symmetric second-order discretization in the current CFD implementation. The corresponding truncation error involves third and higher-order derivatives of velocity, pressure and temperature. On integration over a finite volume cell, the error term thus involves integration of these higher order derivatives. The leading error term scales as $1/\delta^3$, where δ is the computed shock thickness, and hence the error takes large values in the region of a flow discontinuity. When all the finite volume cells spanning the shock wave are taken together, these error terms from the individual cells add up and appear as numerical internal volume sources. Their overall contribution across the shock wave therefore involves higher-order velocity, pressure and temperature derivatives evaluated in the region of flow discontinuity. Unlike the conservative flux terms, the telescopic effect of error cancellation between adjacent cells is absent in the non-conservative source terms. This leads to errors that are comparable or larger than the physical production at the shock waves. Also, the numerical error at shock waves does not decrease in magnitude with successive grid refinements as observed for smooth solutions.

The characteristic of the numerical error obtained in simulations using non-conservative shock-unsteadiness k-ϵ model is reported in Sinha et al. [29]. Non-conservative nature of the source terms causes non-physical trends in the k and ϵ_s amplifications. In particular, the computed TKE amplification shows a non-monotonic trend with increasing Mach number, which is in contrast to the variations observed in DNS and LIA. The results are also qualitatively and quantitatively different from the exact integration of the governing equations. To restrict the truncation errors at shock waves, Sinha et al. [29] proposes an alternative form of the shock-unsteadiness k-ϵ equations obtained by a transformation of the turbulence variables. Conserved quantities involving k and ϵ are formulated and transport equations for these new variables are derived. These new turbulence model equations are free of the non-conservative source terms and show dramatic improvement in numerical accuracy. Here, we follow a similar approach for Eqs. (8) and (15) to derive the corresponding conservative forms.

4.4. *Conservative formulation*

From Eq. (10), we can write $k_2 u_2^{2/3} p_2^{2c/3} = k_1 u_1^{2/3} p_1^{2c/3}$ such that the quantity

$$f = k u^{2/3} p^{2c/3} \tag{18}$$

is conserved across the shock. A transport equation for f can be derived by differentiating f w.r.t. x,

$$\begin{aligned} \rho u \frac{\partial f}{\partial x} &= \rho u^{2/3+1} p^{2c/3} \frac{\partial k}{\partial x} + \frac{2}{3}\rho k u^{2/3} p^{2c/3} \frac{\partial u}{\partial x} \\ &\quad + \frac{2}{3} c \rho k u^{2/3+1} p^{2c/3-1} \frac{\partial p}{\partial x} \end{aligned} \tag{19}$$

Note that from now onwards, the overbars on ρ and p and tilde on u and T are dropped to avoid potential conflict with the sign of the exponent. Multiplying the TKE equation (8) by $u^{2/3} p^{2c/3}$, we get

$$\begin{aligned} \rho u^{2/3+1} p^{2c/3} \frac{\partial k}{\partial x} &= -\frac{2}{3}\rho k u^{2/3} p^{2c/3} \frac{\partial u}{\partial x} - \frac{2}{3} c \rho k u^{2/3+1} p^{2c/3-1} \frac{\partial p}{\partial x} \\ &\quad - \rho \epsilon_s u^{2/3} p^{2c/3} \end{aligned} \tag{20}$$

Table 2: Normalized values of k and ϵ at the inlet station for different Mach number cases.

M	$k_0 \times 10^2$	$\epsilon_0 \times 10^4$	DNS source
1.5	2.88	11.3	Larsson and Lele [36]
2.0	2.76	10.7	–
2.5	2.69	10.4	Larsson and Lele [36]
2.75	2.66	10.3	–
3.0	2.64	10.2	–
3.5	2.61	10.0	Larsson and Lele [36]
4.25	2.57	9.9	–
4.7	2.56	9.8	Larsson and Lele [36]

which on substituting in Eq. (19) and using mass conservation across the shock, we get

$$\frac{\partial}{\partial x}(\rho u f) = -\rho\epsilon_s u^{2/3} p^{2c/3} \tag{21}$$

This equation is mathematically identical to the TKE equation (8), but the source terms with non-conservative derivative have been eliminated. Due to this, the corresponding discretization error exhibits a telescoping effect at the cell interfaces. We thus get a well-behaved numerical solution at a flow discontinuity, as shown in the results.

Similarly, from Eq. (16), the conserved quantity across the shock turns out to be

$$g = u^{c_w - 1}\epsilon_s T^{-\alpha} \tag{22}$$

and the corresponding transport equation is

$$\frac{\partial}{\partial x}(\rho u g) = -c_2\rho\frac{\epsilon_s^2}{k}u^{c_w-1}T^{-\alpha} \tag{23}$$

Substituting $\epsilon_s = g u^{1-c_w}T^{\alpha}$ and $k = f u^{-2/3}p^{-2c/3}$, Eqs. (21) and (23) can be cast into the following form :

$$\frac{\partial}{\partial x}(\rho u f) = -\rho g(u^{\frac{5}{3}-c_w}T^{\alpha}p^{2c/3}) \tag{24}$$

$$\frac{\partial}{\partial x}(\rho u g) = -c_2\rho\frac{g^2}{f}(u^{\frac{5}{3}-c_w}T^{\alpha}p^{2c/3}) \tag{25}$$

The above equations are similar to the original Eqs. (8) and (15), except for the absence of the production terms. The dissipation terms retain their original form with an additional factor of $(u^{\frac{5}{3}-c_w}T^{\alpha}p^{2c/3})$.

5. Simulation Methodology

The one-dimensional Reynolds-averaged Navier-Stokes equations are solved for the mean flow and the newly proposed form of k-ϵ model is used for turbulence closure. The diffusive fluxes are not included in the computation because their contribution is expected to be small in the current shock-turbulence interaction. All the equations are solved in their non-dimensional form. The dimensionless and normalized quantities are defined as :

$$\begin{array}{lll} x = x^*\kappa_0 & t = t^*/(1/a^*_\infty\kappa_0) & u = u^*/a^*_\infty \\ \rho = \rho^*/\rho^*_\infty & p = p^*/(\rho^*_\infty a^{*2}_\infty) & T = T^*/T^*_\infty \\ R = R^*/(\gamma R^*) & k = k^*/a^{*2}_\infty & \epsilon = \epsilon^*/(a^{*3}_\infty\kappa_0) \end{array}$$

where $(.)^*$ represent quantities in their dimensional form and $(.)_\infty$ represent the corresponding free-stream values. Here, a is the mean speed of sound, $\gamma = 1.4$ and $R = 287.1$ J/kg.K is the specific gas constant. The most energetic wave number $\kappa_0 = 4\ m^{-1}$ in the incoming turbulence field is taken as the characteristic length scale.

A finite-volume approach is used to solve the mean conservation equations fully coupled with the k-ϵ model equations. The system of governing equations in the conservation form can be written as,

$$\frac{\partial}{\partial t}\underbrace{\begin{Bmatrix}\rho\\ \rho u\\ E\\ \rho f\\ \rho g\end{Bmatrix}}_{[U]} + \frac{\partial}{\partial x}\underbrace{\begin{Bmatrix}\rho u\\ \rho u^2 + p + (2/3)\rho u^{-2/3}p^{-2c/3}f\\ (E+p)u + (2/3)\rho u^{1/3}p^{-2c/3}f\\ \rho u f\\ \rho u g\end{Bmatrix}}_{[F]} = \underbrace{\begin{Bmatrix}0\\ 0\\ 0\\ -\rho g(u^{\frac{5}{3}-c_w}T^{\alpha}p^{2c/3})\\ -c_2\rho g^2(u^{\frac{5}{3}-c_w}T^{\alpha}p^{2c/3})/f\end{Bmatrix}}_{[S]} \tag{26}$$

Here, [U] is the vector of conserved variables, [F] is the vector containing inviscid fluxes and [S] is the vector containing the source terms. The total mean energy E is given by,

$$E = \frac{p}{(\gamma-1)} + \frac{1}{2}\rho u^2 + \rho u^{-2/3}p^{-2c/3}f \tag{27}$$

The non-conservative form of k-ϵ equations given by Eqs. (8) and (15) can also be written in a form similar to Eq. (26). The equations are integrated using the conservation form of Lax-Friedrichs scheme. A fixed CFL value of 0.2 is used for all the computations, which renders the scheme to be first order accurate in space and time. The turbulent source terms are evaluated at the cell centers. In case of the simulations of nonconconservative form of the turbulence equations, the velocity, pressure and temperature gradients in the production terms are discretized using a second-order accurate central difference scheme. Explicit time integration is achieved using the first order forward Euler method. The code has been successfully used to reproduce the results from [29], which were obtained using Steger-Warming flux-vector splitting method. However, Lax-Friedrichs scheme requires more number of grid points to obtain identical results for a particular Mach number when compared with the code used in [29].

The mean flow Mach number for the test cases range from low supersonic to nearly the hypersonic limit. DNS data for a limited number of cases are presented by Larsson and Lele [36], where the turbulent Mach number M_t, defined as $M_t^2 = 2k^*/a^{*2}$, immediately upstream of the shock wave is 0.22. The Reynolds number based on Taylor microscale Re_λ is 40 at this location. The computational domain ranges from $x = -7.6$ to $x = 29.6$. The normalized value of TKE just upstream of the shock is calculated as

$$k_1 = \frac{M_t^2}{2} \tag{28}$$

The Taylor microscale is given by $\lambda^* = \sqrt{10\nu^* k^*/\epsilon^*}$ and the Reynolds number based on Taylor microscale is defined as $Re_\lambda = \lambda^* u_{rms}^{'*}/\nu^*$ [46]. For homogeneous-isotropic turbulence, we have $u_{rms}^{'*} = \sqrt{2k^*/3}$. Using these relations, the normalized value of turbulence dissipation rate immediately upstream of shock can be calculated as

$$\epsilon_1 = \frac{5}{\sqrt{3}}\left(\frac{M_t^3}{\kappa_0\lambda^*}\right)\frac{1}{Re_\lambda} \tag{29}$$

Using a non-dimensional value of Taylor microscale $\kappa_0\lambda^* = 0.84$, we get $k_1 = 0.0242$ and $\epsilon_1 = 9.15 \times 10^{-4}$. Upon solving the equations for homogeneous isotropic turbulence governing the evolution of k and ϵ from the inlet station to the shock location (for more details, see Appendix), we get the relations for the inlet values of the turbulence variables in their normalized form as

$$\frac{k_0}{\epsilon_0} = \frac{k_1}{\epsilon_1} - t_{sh} \quad , \quad \epsilon_0 = \epsilon_1\left[1 + \frac{t_{sh}}{\left(\frac{k_1}{\epsilon_1} - t_{sh}\right)}\right]^{\frac{c_{\epsilon 2}}{c_{\epsilon 2}-1}} \tag{30}$$

where, $t_{sh} = (c_{\epsilon 2} - 1)x_{sh}/u_1$, $c_{\epsilon 2} = 1.2$ and $x_{sh} = 6.83$ is the shock location from the inlet. The canonical shock-turbulence interaction flows computed in this work are listed in Table 2. The values of k_0 and ϵ_0 for all the cases are obtained by using Eq. (30) with the conditions just upstream of the shock taken from DNS of Larsson and Lele [36]. Free-stream and inlet conditions are specified at the upstream boundary. Rankine-Hugoniot jump relations are used to set-up the shock at $x = 0$. For the exit boundary, a Neumann condition of the form $\frac{\partial}{\partial x}[U_{exit}] = 0$ is employed, where $[U_{exit}]$ is the vector of conserved variables at the exit.

The original CFD code is based on the non-conservative form of k and ϵ equations (8) and (15). Like Sinha et al. [29], the conservative form of the model Eqs. (24) and (25) can be easily incorporated by interpreting the turbulence variables in the code as f and g, instead of k and ϵ. Minimal changes are then required to the CFD code to implement the conservative form of the k-ϵ equations. These are listed next.

1. The initial and boundary conditions for k and ϵ are transformed to the new variables f and g as per Eqs. (18) and (22).
2. Computation of the turbulent source terms are modified by dropping the production terms and multiplying the dissipation term by a factor $(u^{5/3-c_w}T^\alpha p^{2c/3})$.
3. The pressure is calculated from the total mean energy Eq. (27), which requires numerically solving the algebraic non-linear equation,

$$p + (\gamma - 1)fu^{-2/3}p^{-2c/3} = (\gamma - 1)\left(E - \frac{1}{2}\rho u^2\right) \tag{31}$$

   at the end of each time step. In this work, Secant method is used and it takes three iterations to get the pressure at each grid point for all the upstream Mach number cases considered.
4. The original turbulence variables k and ϵ are then recovered from the converged flowfield solution by invoking the reverse transform as per Eqs. (18) and (22).

6. Simulation Results and Discussion

6.1. Grid Refinement Study

The non-conservative and the conservative forms of the new k-ϵ model are subjected to a grid refinement study. A test case with upstream Mach number of 2.5 is chosen and the results are computed using three grids : baseline grid of 1600 points, a finer grid of 3200 points and a coarser grid with 800 points. Grid points are uniformly distributed between the inlet and exit locations, such that the shock normal grid spacing for the three grids are 4.65×10^{-2}, 2.325×10^{-2} and 1.1625×10^{-2} respectively. Note that the x-coordinate is normalized by the most energetic wave number in the upstream turbulence field.

Fig. 7 shows the variation of k and ϵ along the streamwise direction, where the turbulence quantities are normalized by their values immediately upstream of the shock wave. It is found that the variation in grid-point density has noticeable effect on the k and ϵ solutions in the shock region. The thickness of the shock decreases on successive grid refinement, and we see an increase in the k and ϵ amplification. The pre and post-shock decays are relatively insensitive to grid refinement for both the conservative and non-conservative formulations of the proposed k-ϵ model. Overall, the baseline grid of 1600 points is found to be adequate for the Mach 2.5 case considered here, and is used in the majority of comparisons presented in this section. The non-conservative k-ϵ model solution is more sensitive to grid-point density at higher Mach numbers, as discussed next.

The amplification in turbulent dissipation rate as computed using the non-conservative Eq. (15) is plotted as a function of upstream Mach number in Fig. 8a. The exact solution (16) obtained by analytical integration of the equation is also shown for comparison. The numerical solution is much higher than the exact integration for Mach numbers beyond 2; note the log scale used for the vertical axis. Further, the amplification increases with grid refinement and does not show a converging trend. This is due to the increase in the truncation error in the ϵ-equation with grid refinement. The leading velocity and temperature derivatives in the error term have $1/\delta^3$ variation, as discussed earlier. This scales as $1/\Delta x^3$, since δ is proportional to the grid size Δx. Thus, for a fixed Mach number, the amplification in turbulent dissipation rate increases with grid refinement.

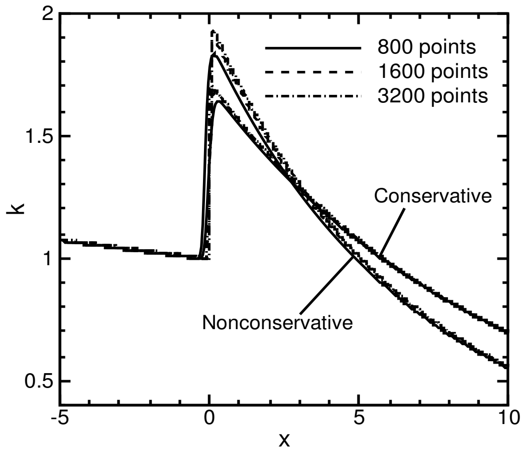

(a)

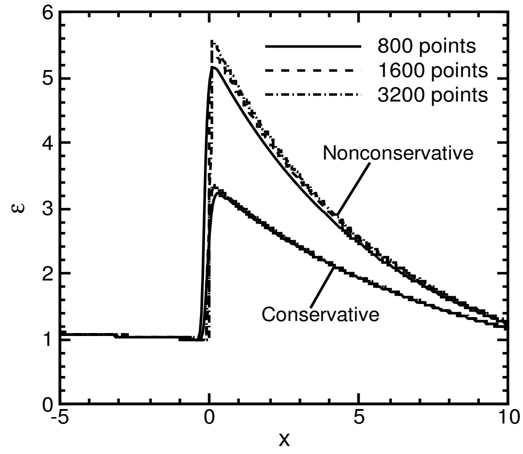

(b)

Figure 7: Effect of grid refinement on (a) TKE and (b) turbulent dissipation rate evolution for upstream Mach number of 2.5.

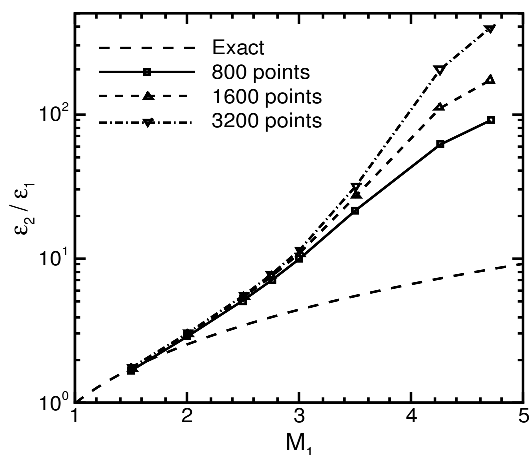

(a)

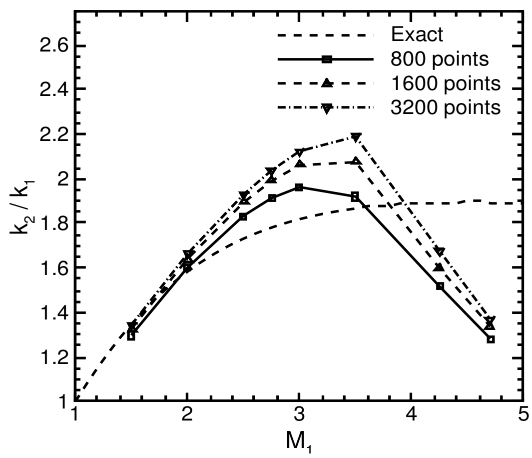

(b)

Figure 8: Amplification in (a) ϵ and (b) k computed using the non-conservative k-ϵ equations on successively refined grids for a range of upstream Mach number.

Similarly, owing to the large discretization errors due to the non-conservative production terms in the k-equation (8), the numerical results over-predict the exact inviscid integration (10). For a fixed Mach number, the TKE amplification also increases on successive grid refinement for Mach numbers up to about 3. At higher Mach numbers, the numerical prediction is lower than the exact solution. Further, the TKE amplification decreases with increasing shock strength, which is opposite to what is observed for the turbulent dissipation rate and is physically unrealistic. This behaviour is similar to that observed in [29] and is due to very high amplification of the turbulent dissipation rate for high Mach numbers.

On the other hand, the TKE and dissipation rate amplifications obtained using the conservative equations (Fig. 9) show a converging behaviour as the grid is successively refined. The solutions are also consistent with the exact integration results. This improvement in the results over the non-conservative case is due to the reason that the conservative formulation removes the non-conservative source terms, which causes large discretisation errors. The truncation error in the convective terms scales as $(\Delta x)^2$, and hence decreases as the grid spacing is reduced. The 1600 and 3200 grids yield close results, and it can be seen that, in the limit of $\Delta x \to 0$, the numerical results will approach the exact inviscid integration results.

6.2. Comparisons with DNS

We next evaluate the accuracy of the proposed turbulence model equations, both the conservative and non-conservative formulations. The results are compared with the DNS data of Larsson et al. [36] and conservative form of shock-unsteadiness k-ϵ model [29]. We note that the k-ϵ model proposed in [29] is based on the physics-based shock-unsteadiness correction of Sinha et al. [24] and is cast in a conservative form to eliminate numerical errors at shock discontinuities. It has been shown to match the DNS data well in the previous work. By comparison, the current k-ϵ model emulates the physics of the shock-unsteadiness model with constant turbulence model parameters. This is unlike the [29] model which has model parameters as

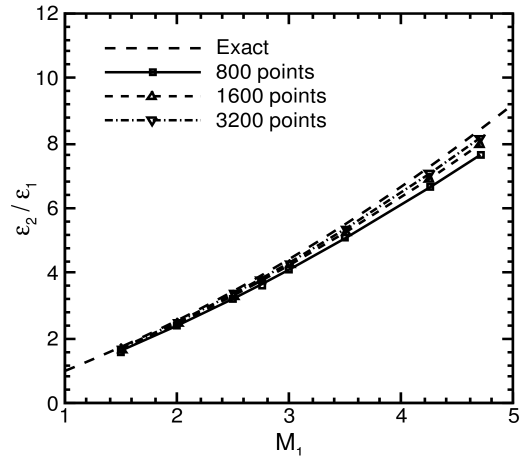

(a)

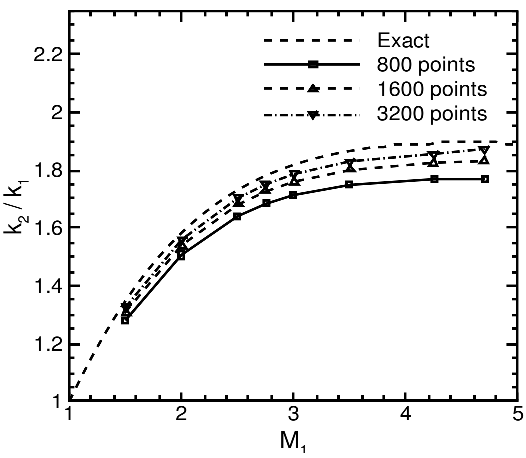

(b)

Figure 9: The conservative k-ϵ equations show a systematic grid convergence in (a) ϵ and (b) k amplifications for all Mach numbers.

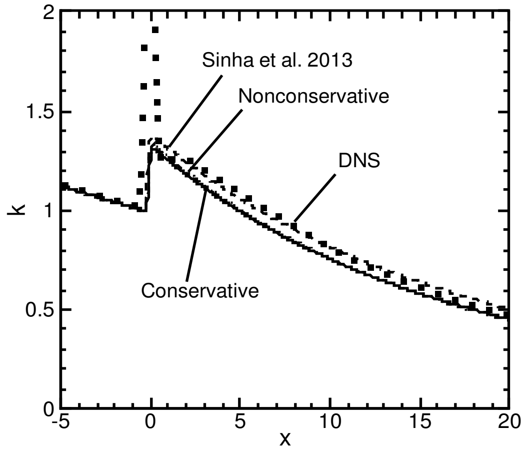

(a)

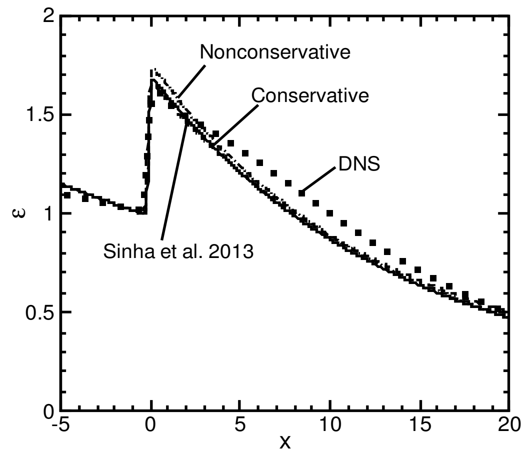

(b)

Figure 10: Streamwise variation of TKE and turbulent dissipation rate in the Mach 1.5 shock/homogeneous turbulence interaction shows that all model predictions are comparable to the DNS data.

function of the upstream Mach number, and hence lead to difficulty in CFD implementation for complex STBLI flows.

Evolutions of TKE and its dissipation rate along the streamwise direction are plotted for different upstream Mach numbers in Figs. 10 - 12. As earlier, the TKE and dissipation rate are normalized by their values just before the shock wave, and the simulations are performed using 1600 grid points. The TKE and dissipation rate profiles show decay on either sides of the shock and amplifications in their values can be seen only in the shock region. This is because the production of TKE is due to the mean velocity and mean pressure gradients, and the production of dissipation rate is due to the mean velocity and mean temperature gradients. The DNS data also shows high values of TKE at the shock. These are due to unsteady shock oscillations, and are not captured by the turbulence models.

The pre-shock decay of TKE and dissipation rate for the three test cases obtained using all the k-ϵ models match well with the DNS data. For the Mach 1.5 case, in Fig. 10, the model predictions match the DNS amplification of k and ϵ fairly well, with minor discrepancies in the post-shock evolution of the turbulence field. As noted earlier, the current model slightly underpredicts the TKE amplification as compared to [29] and DNS data at this Mach number. Further, both the conservative and non-conservative forms yield practically identical solutions for such weak shock interactions. There is a slight overprediction of the turbulent dissipation rate amplification by the non-conservative equations, as compared to the conservative form.

The effect of the numerical errors due to the non-conservative production terms in the model equations is prominent in the higher Mach number cases. The non-conservative amplification of turbulent dissipation rate dramatically increases with Mach number. It is higher by about 67% at Mach 2.5, whereas for the M = 3.5 case, the overprediction is over 425%. The TKE amplifications are also overpredicted for these cases (see Figs. 11 and 12). The excessive amplification of ϵ across the Mach 3.5 shock results in a steeper decay of both TKE and dissipation rate in the downstream flow. The turbulence quantities drop to negligible values behind the shock wave. Thus, the post-shock

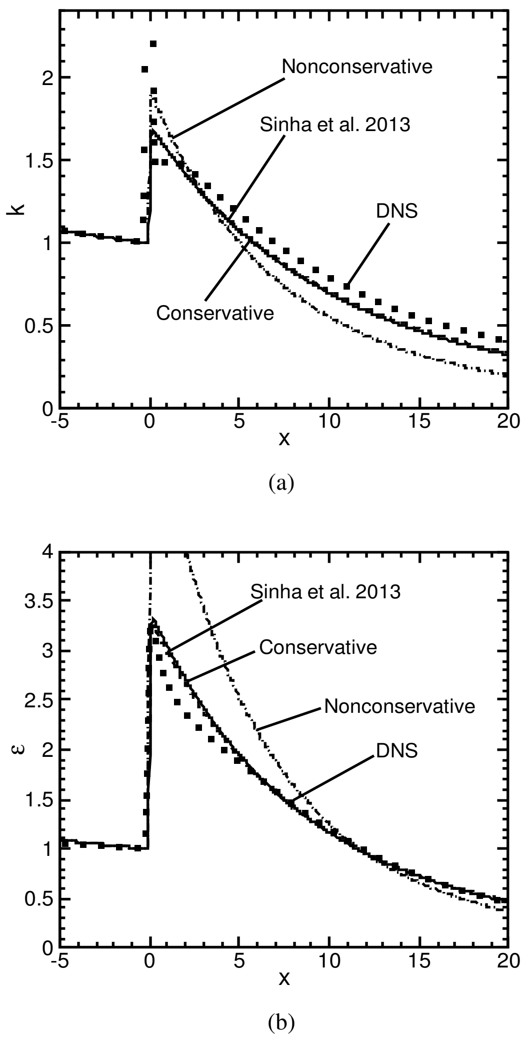

Figure 11: Spatial evolution of TKE and turbulent dissipation rate in the shock/homogeneous turbulence interaction for $M_1 = 2.5$.

TKE and dissipation rate for the non-conservative equations are in complete disagreement with the results obtained using the conservative form, Sinha et al. [29] and DNS. The discrepancy increases with shock strength, and is because of the large numerical errors caused due to the non-conservative derivatives present in the model equations.

The numerical results obtained using the conservative form of the proposed k-ϵ turbulence model are in excellent agreement with the physics-based model developed previously [24, 29]. Both the amplification across the shock and the downstream decay match DNS data closely at Mach 2.5 (Fig. 11). For the Mach 3.5 case (Fig. 12), the shock-jumps in k and ϵ are reproduced accurately, but the dissipation rate is over-predicted in the region $0 < x < 10$. This results in a faster decay of TKE behind the shock in this region. Further downstream, the conservative model Eqs. (24) and (25) predict a lower TKE than DNS, but the decay rate seems to match the DNS data well.

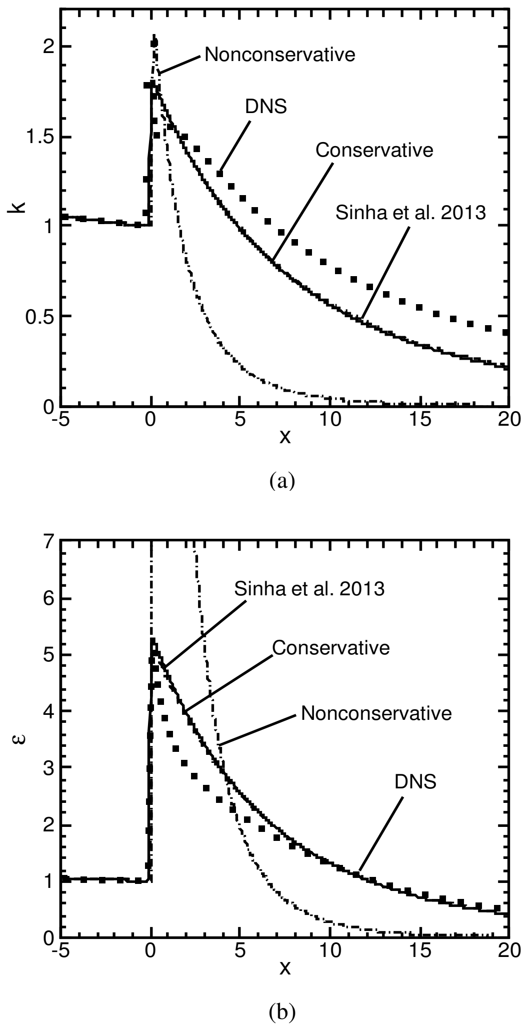

Figure 12: Streamwise variation of TKE and turbulent dissipation rate in the shock/homogeneous turbulence interaction for $M_1 = 3.5$.

7. Extension to realistic flows

For application to realistic flows involving shock waves, the model equations (8) and (15) can be cast in a general tensor form as,

$$\frac{\partial \rho k}{\partial t} + \frac{\partial \rho u_j k}{\partial x_j} = -\frac{2}{3}\rho k \frac{\partial u_i}{\partial x_i} - \frac{2}{3} c \rho k \frac{u_i}{p}\frac{\partial p}{\partial x_i} - \rho\epsilon \tag{32}$$

$$\frac{\partial \rho \epsilon}{\partial t} + \frac{\partial \rho u_j \epsilon}{\partial x_j} = (1 - c_w)\rho\epsilon \frac{\partial u_i}{\partial x_i} + \alpha\rho\epsilon \frac{u_i}{T}\frac{\partial T}{\partial x_i} - c_2 \rho \frac{\epsilon^2}{k} \tag{33}$$

where we drop overbars and tilde, assume $\epsilon \simeq \epsilon_s$ and the temporal derivative is introduced for unsteady flows. The equations have a form similar to the mean flow equations, and they can be solved either coupled or decoupled in a RANS code. It can be shown that the above equations are invariant under rotation of the co-ordinate axes. The conservative formulation in Eqs. (24) and (25) can also be generalized in a similar way, by replacing the velocity dependence of the right-hand-side terms by equivalent expressions involving fluid density.

For turbulence interacting with an oblique shock, Eqs. (32) and (33) are written in a rotated co-ordinate frame such that the shock-normal direction coincides with the $x^{'}$ - axis,

$$\frac{\partial \rho k}{\partial t} + \frac{\partial \rho u_n k}{\partial x^{'}} = -\frac{2}{3}\rho k \frac{\partial u_n}{\partial x^{'}} - \frac{2}{3} c \rho k \frac{u_n}{p}\frac{\partial p}{\partial x^{'}} - \rho \epsilon \tag{34}$$

$$\frac{\partial \rho \epsilon}{\partial t} + \frac{\partial \rho u_n \epsilon}{\partial x^{'}} = (1 - c_w)\rho\epsilon \frac{\partial u_n}{\partial x^{'}} + \alpha\rho\epsilon \frac{u_n}{T}\frac{\partial T}{\partial x^{'}} - c_2 \rho \frac{\epsilon^2}{k} \tag{35}$$

where u_n is the shock-normal velocity component and the shock-parallel derivatives are neglected. The above equations have the same form as Eqs. (8) and (15), and thus the oblique-shock interaction is equivalent to a normal shock interaction in the shock-normal direction.

Integrating the above equations across the shock wave, we get amplifications in k and ϵ as,

$$\left(\frac{k_2}{k_1}\right) = \left(\frac{\rho_2}{\rho_1}\right)^{2/3} \left(\frac{p_2}{p_1}\right)^{-2c/3} \tag{36}$$

$$\left(\frac{\epsilon_2}{\epsilon_1}\right) = \left(\frac{\rho_2}{\rho_1}\right)^{c_w - 1} \left(\frac{T_2}{T_1}\right)^{\alpha} \tag{37}$$

where $\rho_1 u_{n,1} = \rho_2 u_{n,2}$ across the shock is used. Similarly, the amplifications in k and ϵ across an oblique shock for the shock-unsteadiness k-ϵ model is given by,

$$\left(\frac{k_2}{k_1}\right) = \left(\frac{\rho_2}{\rho_1}\right)^{\frac{2}{3}(1-b_1^{'})} \tag{38}$$

$$\left(\frac{\epsilon_2}{\epsilon_1}\right) = \left(\frac{\rho_2}{\rho_1}\right)^{(2/3)c_{\epsilon 1}} \tag{39}$$

Fig. 13 plots the amplifications in TKE and turbulent dissipation rate across weak oblique shocks for varying flow deflection angles θ and upstream Mach numbers M_1. The results are presented for a range of upstream Mach numbers up to 5 and the solutions are obtained for attached shocks. Detached shock cases are discussed separately. Note that the shock-normal Mach number M_{1n} is considerably lower than M_1 for oblique shocks with low deflection angles. This suggests that the model predictions are valid over a much larger range of upstream Mach numbers than that presented in Fig. 13. For $\theta = 15^o$, for example, hypersonic flows up to Mach 15 fall within the calibration range $1 \le M_{1n} \le 5$ considered in Section 4.1.

For a given deflection angle θ, TKE amplification increases with increasing Mach number (Fig. 13a). The current model gives qualitatively the same trend as the shock-unsteadiness k-ϵ model, but the predictions are lower in magnitude. The largest differences observed for $\theta = 15^o$ and $M_{1n} \simeq 2$ - 3 are within the 5% margin reported in Table 1. The two models are closer at higher deflection angles, where TKE amplification tends to approach its hypersonic asymptotic value. The ϵ-data presented in Fig. 13b also shows a close match between the current model and the shock-unsteadiness $k - \epsilon$ model for weak oblique shocks. The current predictions are higher than those of the previous model for all Mach numbers and flow deflection angles with a maximum difference of about 3.5%.

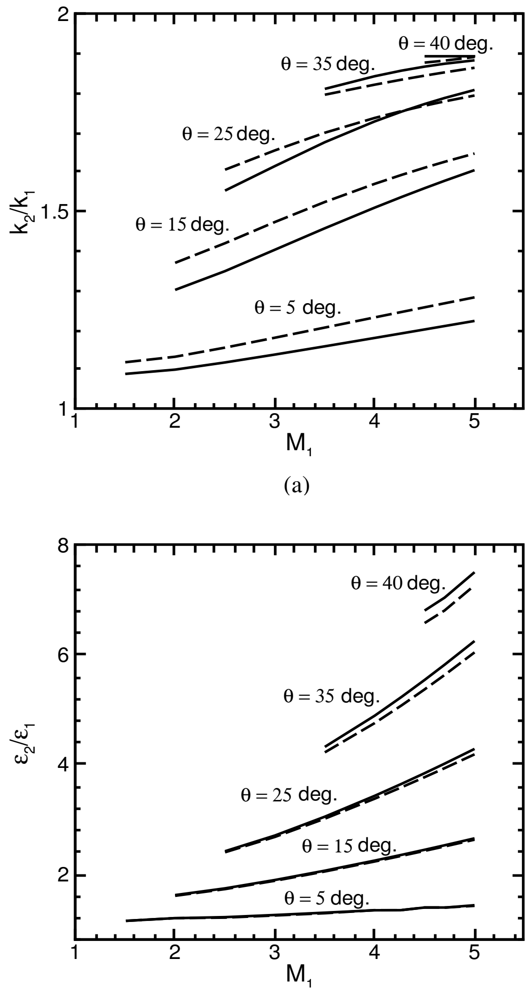

(b)

Figure 13: Amplifications in (a) TKE and (b) turbulent dissipation rate across weak oblique shocks obtained using the present model (solid lines) and the shock-unsteadiness k-ϵ model (dashed lines).

In case of strong oblique shocks, the model predictions for different flow deflection angles are close to each other. The k and ϵ amplifications are also comparable to the normal shock results presented in Figs. 5 and 6, and are not repeated here. As expected, the differences between the current model and the shock-unsteadiness k-ϵ model predictions are well within 5% for all Mach numbers and flow deflection angles considered.

The model prediction in realistic flows with Mach stems and lambda shocks [3, 47] would be as per the results shown for normal and oblique shocks, respectively. In case of STBLI flows, the mean flow gradients in the upstream boundary layer results in a curved shock with strength varying with distance from the wall. Application of the generalized model equations (32) and (33) would give turbulence amplification as per the local strength and inclination of the shock wave. The k and ϵ results would follow the M_1 - θ dependence presented in Fig. 13. Also, the model should be restricted to the supersonic part of a boundary layer, and not applied to the near-wall subsonic region where shock waves cannot penetrate.

Implementation of the current model in realistic flow simulations require a shock-identifying function, such that the model is applied in high-compression regions and we revert back to the standard turbulence model outside of shock waves. A function based on the mean dilatation has proved effective for the shock-unsteadiness model applied to different STBLI configurations at varying Mach numbers [9, 16]. See, for example, the impingement of an oblique shock on a flat plate boundary layer, where the shock-unsteadiness model is applied in regions covered by the incident and transmitted shocks, as well as the separation and reattachment shock waves [28]. Implementation of the proposed model in a general CFD code will follow identical steps with appropriate modification required for the pressure and temperature gradient terms. A detailed validation of the model against experimental data for different geometric configurations, with varying freestream and wall boundary conditions, is beyond the scope of the present investigation.

The behaviour of the current model is expected to be similar to the shock-unsteadiness model, which suppresses turbulent kinetic energy amplification at shock waves. A lower turbulence at the separation shock leads to an early separation of the turbulent boundary layer [28], and thus alleviates one of the key limitation of standard k-ϵ models [1, 2]. Matching the separation bubble size leads to an accurate prediction of the shock topology in the interaction region [16], including the location and inclination of different shocks, as well as their interaction with each other. The simulations are thus able to predict the experimental data for surface pressure and skin friction coefficient better than conventional models [9]. Improvements in wall heating rates, however, are limited, and require additional modeling as proposed in recent works [48, 49]. Overall, the models based on shock-unsteadiness damping have proved their potential in a variety of STBLI configurations in supersonic and hypersonic flows. The results are also consistent across different one- [41] and two-equation turbulence models [16], and the same is expected for the new k-ϵ model proposed in this paper.

8. Conclusion

This paper presents a physically sound and numerically robust k-ϵ model for application to high-speed turbulent flows with shock waves. A new physically-consistent source term is proposed to model the shock-unsteadiness damping of turbulent kinetic energy. The turbulent dissipation rate equation is based on the physical effects of mean compression and enhancement of fluid viscosity across a shock wave. Unlike previous physics-based turbulence models, the current model parameters are independent of the shock strength and hence do not require prior knowledge of the upstream mean flow Mach number. This can be of significant advantage while applying the model equations to realistic flows with multiple shock waves and their interaction with boundary layers. The model equations are also cast in a conservative form so as to eliminate numerical error at flow discontinuities. The model is tested extensively in canonical shock-turbulence interaction and found to match available DNS data well over a range of Mach numbers. The superior numerical characteristics, in terms of grid convergence of the solution, is also demonstrated. Overall, the present study shows the enhanced potential of the proposed k-ϵ model equations and provides the basis for further application to shock-boundary layer interaction flows.

Acknowledgement

The authors would like to acknowledge the contributions of Mr. Kishan Kumar, a summer intern at IIT Bombay, towards the initial development of the model equations.

Appendix

For steady one-dimensional uniform mean flow upstream of the shock wave, the variations in k and ϵ are governed by,

$$u_1 \frac{\partial k}{\partial x} = -\epsilon \tag{A.1}$$

$$u_1 \frac{\partial \epsilon}{\partial x} = -c_{\epsilon 2} \frac{\epsilon^2}{k} \tag{A.2}$$

The above equations are in non-dimensional form and the respective characteristic quantities used for non-dimensionalization are mentioned in Section 5. These equations are obtained by neglecting the production terms from Eqs. (8) and (15), as there is no gradient in the mean velocity in this region. Also, the velocity is constant in this region and is equal to u_1, where $u_1 = M_1$ because of the non-dimensionalization considered. The tilde over u_1 is neglected and $\epsilon_s \simeq \epsilon$ is taken. Eqs. (A.1) and (A.2) can be written as,

$$\frac{\partial \epsilon}{\epsilon} = c_{\epsilon 2} \frac{\partial k}{k} \tag{A.3}$$

On integration, we get

$$\epsilon = k^{c_{\epsilon 2}} C \tag{A.4}$$

where C is the integration constant. Substituting in Eq. (A.1) and integrating along x, we get

$$k = \left[\frac{(Cx + \hat{C})}{u_1} (c_{\epsilon 2} - 1) \right]^{-\frac{1}{c_{\epsilon 2} - 1}} \tag{A.5}$$

where $\hat{C}$ is another integration constant.

Using the boundary condition $k = k_0$ and $\epsilon = \epsilon_0$ at $x = 0$, we get

$$\hat{C} = \frac{u_1 k_0^{c_{\epsilon 2} - 1}}{c_{\epsilon 2} - 1} \qquad \text{and} \qquad C = \epsilon_0 k_0^{-c_{\epsilon 2}} \tag{A.6}$$

and thus

$$k(x) = k_0 \left[1 + \frac{\epsilon_0}{k_0} \frac{x(c_{\epsilon 2} - 1)}{u_1} \right]^{-\frac{1}{c_{\epsilon 2} - 1}} \tag{A.7}$$

The expression for the turbulent dissipation rate can be obtained using Eq. (A.1) as,

$$\epsilon(x) = \epsilon_0 \left[1 + \frac{\epsilon_0}{k_0} \frac{x(c_{\epsilon 2} - 1)}{u_1} \right]^{-\frac{c_{\epsilon 2}}{c_{\epsilon 2}-1}} \tag{A.8}$$

The above equations give the variations in k and ϵ from the inlet station to the point just upstream of the shock. Now, if x_{sh} corresponds to the shock location, then at $x = x_{sh}$, $k = k_1$ and $\epsilon = \epsilon_1$. Hence, Eqs. (A.7) and (A.8) can be written in terms of the inlet values as,

$$k_0 = k_1 \left[1 + \frac{\epsilon_0}{k_0} x_{sh} \frac{(c_{\epsilon 2} - 1)}{u_1} \right]^{\frac{1}{c_{\epsilon 2}-1}} \tag{A.9}$$

and

$$\epsilon_0 = \epsilon_1 \left[1 + \frac{\epsilon_0}{k_0} x_{sh} \frac{(c_{\epsilon 2} - 1)}{u_1} \right]^{\frac{c_{\epsilon 2}}{c_{\epsilon 2}-1}} \tag{A.10}$$

The same expressions hold if the shock is at $x = 0$ and x_{shk} is the distance of the shock from the inlet station. In the present work, $x_{shk} = 6.83$ for all the computations performed. Now, given the values of k_1 and ϵ_1 calculated using Eqs. (28) and (29), the inlet values of k and ϵ can be calculated from Eqs. (A.9) and (A.10) as,

$$\epsilon_0 = \epsilon_1 \left[1 + \frac{1}{\left(\frac{k_1}{\epsilon_1} - x_{sh} \frac{(c_{\epsilon 2}-1)}{u_1} \right)} x_{sh} \frac{(c_{\epsilon 2} - 1)}{u_1} \right]^{\frac{c_{\epsilon 2}}{c_{\epsilon 2}-1}} \tag{A.11}$$

and

$$k_0 = \epsilon_0 \left(\frac{k_1}{\epsilon_1} - x_{sh} \frac{(c_{\epsilon 2} - 1)}{u_1} \right) \tag{A.12}$$

It is to note that, in the above expressions, all the quantities are normalized and non-dimensional, with the quantities used for normalization given in Section 5.

References

[1] Hutton AG, Ashworth RM. The challenge of turbulence modelling in modern aeronautical design. Intl. Journal for Numerical Methods in Fluids 2005;47(89):721-37.

[2] Liou WW, Huang G, Shih TH. Turbulence model assessment for shock wave/turbulent boundary-layer interaction in transonic and supersonic flows. Comput Fluids 2000;29(3):275-299.

[3] Balabel A, Hegab AM, Nasr M, El-Behery SM. Assessment of turbulence modeling for gas flow in two-dimensional convergent-divergent rocket nozzle. Applied Mathematical Modelling 2011;35(7):3408-22.

[4] Dimonte G, Tipton R. K-L turbulence model for the self-similar growth of the Rayleigh-Taylor and Richtmyer-Meshkov instabilities. Physics of Fluids 2006;18(8):085101.

[5] Morán-López JT, Schilling O. Multicomponent Reynolds-averaged Navier-Stokes simulations of reshocked Richtmyer-Meshkov instability-induced mixing. High Energy Density Physics 2013;9(1):112-21.

[6] Morán-López JT, Schilling O. Multi-component Reynolds-averaged Navier-Stokes simulations of Richtmyer-Meshkov instability and mixing induced by reshock at different times. Shock Waves 2014;24(3):325-43.

[7] Vieira R, Azevedo JL. RANS simulations of flows with shock wave-boundary layer interaction. 51st AIAA Aerospace Sciences Meeting including the New Horizons Forum and Aerospace Exposition 2013-0985.

[8] Brown JL. Hypersonic shock wave impingement on turbulent boundary layers: Computational analysis and uncertainty. Journal of Spacecraft and Rockets 2013;50(1):96-123.

[9] Sinha K, Mahesh K, Candler GV. Modeling the effect of shock unsteadiness in shock/turbulent boundary-layer interactions. AIAA J 2005;43(3):586-594.

[10] Barakos G, Drikakis D. Assessment of various low-Reynolds number turbulence models in shock-boundary layer interaction. Computer methods in Applied Mechanics and Engineering 1998;160(1):155-74.

[11] Ma L, Lu L, Fang J, Wang Q. A study on turbulence transportation and modification of Spalart-Allmaras model for shock-wave/turbulent boundary layer interaction flow. Chinese Journal of Aeronautics 2014;27(2):200-209.

[12] Morgan B, Duraisamy K, Nguyen N, Kawai S, Lele SK. Flow physics and RANS modelling of oblique shock/turbulent boundary layer interaction. Journal of Fluid Mechanics 2013;729:231-284.

[13] Salin A, Yao Y, Zheltovodov AA. Comparison and improvement of wall heat transfer prediction in crossing-shock-wave/turbulent-boundary-layer interaction conditions. 51st AIAA Aerospace Sciences Meeting including the New Horizons Forum and Aerospace Exposition 2013:666.

[14] Roidl B, Meinke M, Schroder W. A zonal RANS-LES method for compressible flows. Comput Fluids 2012;67: 1-15.

[15] Grilli M, Adams NA, Willems S, Guelhan A. Experimental and numerical investigation on shockwave/turbulent boundary layer interaction. 42nd AIAA fluid dynamics conference and exhibit, American Institute of Aeronautics and Astronautics, New Orleans, Louisiana 2012.

[16] Pasha AA, Sinha K. Simulation of hypersonic shock/turbulent boundary-layer interactions using shock-unsteadiness model. J Prop and Power 2012;28(1):46-60.

[17] Shih TH, Liou WW, Shabbir A, Yang Z, Zhu J. A new k-ϵ eddy viscosity model for high Reynolds number turbulent flows. Comput Fluids 1995;24(3):227-238.

[18] Gaitonde DV. Progress in shock wave/boundary layer interactions. Prog Aerosp Sci 2015;72:80-99.

[19] Zheltovodov AA. Some advances in research of shock wave turbulent boundary layer interactions. AIAA Paper 2006;496:1-25.

[20] Dolling D. Fifty years of shock wave/boundary layer interaction research: what next? AIAA J 2001;39(8):1517-1531.

[21] Loyau H, Batten P, Leschziner MA. Modelling shock/boundary-layer interaction with nonlinear eddy-viscosity closures. Flow, turbulence and combustion 1998;60(3):257-82.

[22] Leschziner MA, Loyau H, Apsley DD. Prediction of shock/boundary-layer interaction with non-linear eddy-viscosity models. CDROM Proceedings of the European Congress on Computational Methods in Applied Sciences and Engineering, CDR Proceedings ECCOMAS 2000.

[23] Barakos G, Drikakis D. Investigation of nonlinear eddy-viscosity turbulence models in shock/boundary-layer interaction. AIAA J 2000;38(3):461-9.

[24] Sinha K, Mahesh K, Candler GV. Modeling shock unsteadiness in shock/turbulence interaction. Phys Fluids 2003;15(8):2290-2297.

[25] Zhang Z, Gao Z, Jiang C, Lee C. Turbulence model modification for fake amplification of Turbulence Kinetic Energy by Shock-Turbulence Interation. In 51st AIAA/SAE/ASEE Joint Propulsion Conference 2015:4205.

[26] Durbin PA. On the k-3 stagnation point anomaly. Int J heat fluid flow 1996;17(1):89-90.

[27] Settles GS, Dodson LJ. Supersonic and hypersonic shock/boundary-layer interaction database. AIAA J 1994;32(7):1377-1383.

[28] Pasha AA, Sinha K. Shock-unsteadiness model applied to oblique shock wave/turbulent boundary-layer interaction. Int J Comput Fluid Dynamics 2008;22(8):569-582.

[29] Sinha K, Balasridhar SJ. Conservative formulation of the k-ϵ turbulence model for shock-turbulence interaction. AIAA J 2013;51(8):1872-1882.

[30] Kovasznay LSG. Turbulence in supersonic flow. Journal of the Aeronautical Sciences 1953;20:657-674.

[31] Lee S, Lele SK, Moin P. Interaction of isotropic turbulence with shock waves: effect of shock strength. J Fluid Mech 1997;340:225247.

[32] Hannappel R, Friedrich R. Direct numerical simulation of a Mach 2 shock interacting with isotropic turbulence. Applied Scientific Research 1995;54(3):205-221.

[33] Lee S, Lele SK, Moin P. Direct numerical simulation of isotropic turbulence interacting with a weak shock wave. J Fluid Mech 1993;251:533-

562.
[34] Mahesh K, Lele SK, Moin P. The influence of entropy fluctuations on the interaction of turbulence with a shock wave. J Fluid Mech 1997;334:353-379.
[35] Jamme S, Cazalbou JB, Torres F, Chassaing P. Direct numerical simulation of the interaction between a shock wave and various types of isotropic turbulence. Flow, Turbulence and Combustion 2002;68(3):227-268.
[36] Larsson J, Lele SK. Direct numerical simulation of canonical shock/turbulence interaction. Phys Fluids 2009;21(12):126101.
[37] Larsson J, Bermejo-Moreno I, Lele SK. Reynolds and Mach number effects in canonical shock-turbulence interaction. J Fluid Mech 2013;717:293-321.
[38] Gatski TB, Bonnet JP. Compressibility, turbulence and high speed flow. Academic Press 2013.
[39] Ribner HS. Convection of a pattern of vorticity through a shock wave. NACA Report 1164 1953.
[40] Veera VK, Sinha K. Modeling the effect of upstream temperature fluctuations on shock/homogeneous turbulence interaction. Phys Fluids 2009;21(2):025101.
[41] Sinha K. Evolution of enstrophy in shock/homogeneous turbulence interaction. J Fluid Mech 2012;707:74-110.
[42] Sinha K, Balasridhar SJ. A conservative turbulence model for shock dominated flows. The 5th European Conference for Aeronautics and Space Sciences, Munich, Germany 1-5 July 2013.
[43] Wilcox DC. Turbulence Modeling for CFD, DCW industries, Inc. 2010 (3rd ed.).
[44] Sarkar S, Erlebacher G, Hussaini M, Kreiss HO. The analysis and modelling of dilatational terms in compressible turbulence. J Fluid Mech 1991;227:473-493.
[45] Haidinger FA, Friedrich R. Computation of shock wave/turbulent boundary layer interactions using a two-equation model with compressibility corrections. Applied Scientific Research 1993;51(1-2):501-505.
[46] Tennekes H, Lumley JL. A first course in turbulence. MIT press 1972.
[47] Hamed A, Vogiatzis C. Overexpanded Two-Dimensional-Convergent-Divergent Nozzle Flow Simulations, Assessment of Turbulence Models. Journal of Propulsion and Power 1997;13(3):444-5.
[48] Quadros R, Sinha K, Larsson J. Turbulent energy flux generated by shock/homogeneous-turbulence interaction. J Fluid Mech 2016;796:113-157.
[49] Quadros R, Sinha K. Modelling of turbulent energy flux in canonical shock-turbulence interaction. *Submitted to* Intl. J. Heat and Fluid Flow 2016.